© 2017. Published by The Company of Biologists Ltd | Journal of Cell Science (2017) 130, 4038-4050 doi:10.1242/jcs.210807

RESEARCH ARTICLE

KIF13A mediates trafficking of influenza A virus ribonucleoproteins

Ana Ramos-Nascimento[1,2], Bárbara Kellen[3], Filipe Ferreira[1], Marta Alenquer[1], Sílvia Vale-Costa[1], Graça Raposo[4], Cédric Delevoye[4] and Maria João Amorim[1,*]

ABSTRACT

Influenza A is a rapidly evolving virus that is successful in provoking periodic epidemics and occasional pandemics in humans. Viral assembly is complex as the virus incorporates an eight-partite genome of RNA (in the form of viral ribonucleoproteins, vRNPs), and viral genome assembly – with its implications to public health – is not completely understood. It has previously been reported that vRNPs are transported to the cell surface on Rab11-containing vesicles by using microtubules but, so far, no molecular motor has been assigned to the process. Here, we have identified KIF13A, a member of the kinesin-3 family, as the first molecular motor to efficiently transport vRNP-Rab11 vesicles during infection with influenza A. Depletion of KIF13A resulted in reduced viral titers and less accumulation of vRNPs at the cell surface, without interfering with the levels of other viral proteins at sites of viral assembly. In addition, when overexpressed and following two separate approaches to displace vRNP-Rab11 vesicles, KIF13A increased levels of vRNP at the plasma membrane. Together, our results show that KIF13A plays an important role in the transport of influenza A vRNPs, a crucial step for viral assembly.

This article has an associated First Person interview with the first author of the paper.

KEY WORDS: KIF13A, Recycling endosome, Influenza A virus assembly, Molecular motor

INTRODUCTION

The influenza A virus (IAV) genome is composed of single-stranded negative-sense RNA and divided into eight independent replication units. Each unit comprises identical RNA termini, of which the 3′ and 5′ ends are partially complementary, and form double-stranded (ds) RNA that accommodates the viral heterotrimeric RNA-dependent RNA polymerase (RdRp) (Pflug et al., 2014). The remainder RNA contains distinct coding regions of variable lengths, coated by nucleoprotein (NP) placed on average every 24 nucleotides (Arranz et al., 2012). In the virion, the eight distinct viral ribonucleoproteins (vRNPs) occupy the inner core and are spatially distinct, with seven segments surrounding a central one in a '7+1' arrangement (Noda and Kawaoka, 2010). Of the, so far, 18 identified proteins that are encoded by the virus (Yamayoshi et al., 2015), only five viral factors – in addition to those forming vRNPs – are essential structural components of the virion. The viral nuclear export protein (NEP) is found attached to vRNPs in modest amounts. Surrounding the genomic core is a layer of the matrix protein 1 (M1) that is coated by a host-derived membrane containing three antigenic viral transmembrane proteins: hemagglutinin (HA), neuraminidase (NA) and matrix protein 2 (M2) (Hutchinson et al., 2014; Shaw et al., 2008).

The mechanisms underlying virion formation inside the host cell are not fully understood. Viral assembly comprises the formation of the supra-molecular complex described above that, at the cell surface, propels viral budding and release. Viral genome complex formation has been reported to be fully dependent on the establishment of RNA–RNA interactions between the different vRNPs (as reviewed in Gerber et al., 2014; Giese et al., 2016; Hutchinson et al., 2010). However, IAV assembly is heavily dependent on host processes, namely for transporting components to the budzone. The transport of the viral transmembrane proteins, HA, NA and M2 to the plasma membrane occurs via the secretory pathway (Doms et al., 1993) and involves the coat protein I (Sun et al., 2013). M1 might be transported along with vRNPs (Noton et al., 2007), M2 (Chen et al., 2008) and/or lipids to the surface, but a detailed analysis of the transport of the M1 pool included in virions is still missing. In the case of vRNPs, the eight-distinct segments are synthesized in the host cell nucleus as independent entities, exported to the cytoplasm (Elton et al., 2001; Ma et al., 2001) and transported to the surface. The endocytic recycling compartment (ERC) was shown to be required for this transport, with vRNPs binding to the major coordinator of ERC trafficking, the GTPase Rab11 (Amorim et al., 2011; Avilov et al., 2012; Eisfeld et al., 2011; Momose et al., 2011). In the healthy cell, Rab11 is switched off or on by binding to GDP or GTP, respectively (Xiong et al., 2012). Activated Rab11 acquires sequential affinity for a series of molecular motors, membrane tethers and v-SNARES, responsible for vesicular movement along cytoskeletal tracks, attachment to and fusion with membranes, respectively (Welz et al., 2014). In relation to molecular motors, Rab11 vesicles were reported to associate with: myosin Vb, dynein light chains 1 and 2, KIF5a and KIF3 of the kinesin-1 and -2 families (Fan et al., 2004; Lapierre et al., 2001; Provance et al., 2008; Roland et al., 2011; Schonteich et al., 2008; Perez Bay et al., 2013; and reviewed in Vale-Costa and Amorim, 2016b). Interestingly, these motors require adaptors for Rab11 binding that belong to the vast family of Rab11-interacting proteins (FIPs) (Horgan and McCaffrey, 2009). Recently, Rab11 vesicles have been shown to associate with an additional motor, KIF13A, from the kinesin-3 family, without recurring to FIPs for binding (Delevoye et al., 2014). During infection, IAV modulates Rab11 trafficking and, as a consequence, this dynamic chain of events is altered. Known effectors of Rab11 are prevented from binding to Rab11 (Vale-Costa et al., 2016), transferrin recycling is reduced (Kawaguchi et al., 2015; Vale-Costa et al., 2016) and FIPs – which are essential components of the pathway – were found to be dispensable for IAV infection (Bruce et al., 2010; Momose et al., 2011). Mechanistically, vRNPs were found to out-compete FIPs for Rab11 binding (Vale-Costa et al.,

[1]Cell Biology of Viral Infection Lab, Instituto Gulbenkian de Ciência (IGC), 2780-156 Oeiras, Portugal. [2]Institute of Virology, Hannover Medical School, 30625 Hannover, Germany. [3]Science4U, MARL Espaços CC02 e CC03, São Julião do Tojal, 2660-421, Loures, Portugal. [4]Institut Curie, PSL Research University, CNRS, UMR144, Structure and Membrane Compartments, 75005 Paris, France.

*Author for correspondence (mjamorim@igc.gulbenkian.pt)

M.J.A., 0000-0002-4129-6659

Received 11 September 2017; Accepted 18 October 2017

Journal of Cell Science (2017) 130, 4038-4050 doi:10.1242/jcs.210807

2016). Therefore, although several papers have confirmed the importance of Rab11 for vRNP delivery to the surface (Amorim et al., 2011; Avilov et al., 2012; Eisfeld et al., 2011; Momose et al., 2011) and for viral assembly (Chou et al., 2013; Lakdawala et al., 2014), it is unclear which host factors are involved in transporting vRNPs to sites of viral assembly. In particular, no molecular motor has been identified as being able to transport vRNP-Rab11 vesicles, and it is unknown if vesicular movement on microtubules is modified by the virus. On the one hand, vRNPs were shown to transit with directed and intermittent movements, at speeds compatible with using microtubule and actin (Amorim et al., 2011; Avilov et al., 2012). Consistent with the usage of the cytoskeleton, NP was shown to colocalize with actin (Avalos et al., 1997; Digard et al., 1999; Roberts and Compans, 1998; Simpson-Holley et al., 2002), and pharmacological destabilization of the microtubule network disrupted shuttling of vRNPs to the plasma membrane (Amorim et al., 2011). On the other hand, drugs acting on actin or microtubule integrity have mild effects in viral production (Amorim et al., 2011; Momose et al., 2007; Simpson-Holley et al., 2002), despite impacting dramatically on virion morphology (Roberts and Compans, 1998; Simpson-Holley et al., 2002). Furthermore, as vRNP binding to Rab11-GTP out-competed the binding of FIPs, it is possible that the vesicular flow is compromised upon infection (Momose et al., 2011; Vale-Costa et al., 2016). In agreement, it has been shown that vRNPs associate with Rab11a ∼300 nm from the nucleus but disassociate ∼500 nm from the cell surface (Nturibi et al., 2017), which indicates that Rab11 is not the final factor delivering vRNPs to the plasma membrane (Eisfeld et al., 2015; Vale-Costa and Amorim, 2016a).

Here, we report that KIF13A positively modulates IAV infection, affecting the trafficking and peripheral localization of vRNPs, but not of the viral transmembrane proteins HA and M2. Depletion of KIF13A did not disturb the initial steps of viral infection, including viral entry, replication and gene expression. Our results suggest a model in which vRNP transport is facilitated by KIF13A on Rab11 vesicles and not by molecular motors that require FIPs for association to Rab11.

RESULTS

KIF13A depletion reduces viral production

To answer whether KIF13A is necessary for IAV infection, we used specific siRNAs to deplete cells of this molecular motor (Fig. 1A-B, Fig. S1), infected or mock-infected cells with influenza A/Puerto Rico/8/34 (hereafter referred to as PR8) and quantified viral production. KIF13A-depleted cells resulted in over 10- and 5-fold reduction in viral titers relative to cells treated with non-targeting siRNAs (siNT) at 6 and 10 hours post infection (hpi), respectively, showing that KIF13A is required for the virus life-cycle (Fig. 1A). When KIF13A mRNA levels were quantified, a consistent average depletion of 80% in mock-infected cells was obtained. In infected cells, depletion was not as efficient, averaging 70% and 60% reduction at 6 and 10 hpi, respectively. Interestingly, infection specifically targets KIF13A for depletion, especially at late stages, as, at 10 hpi, cells treated with non-targeting siRNAs consistently exhibited a 60% decrease in the transcription of KIF13A (Fig. 1B). The significance of this has not been explored further but suggests a virally induced restriction in the amount of KIF13A. Endogenous levels of KIF13A protein were just above the detection limit and depletion was difficult to quantify (Fig. S1A). Western blot analysis showed no detectable differences in viral protein synthesis (Fig. 1C,D) between the two siRNA-treated samples in the times analysed. Our results suggest that KIF13A does not affect the initial steps of viral infection, since viral protein synthesis is similar in cells with and without KIF13A. To evaluate levels of knocked down KIF13A protein, we transfected GFP, GFP-tagged full-length KIF13A (GFP-KIF13A-WT) or an siRNA-resistant GFP-KIF13A form, and treated cells concomitantly with specific RNAs (non-targeting or KIF13A-specific RNAs), and observed that depletion of KIF13A protein was very efficient (Fig. S1B).

Our results indicate that KIF13A is required for the IAV lifecycle, at a step that is downstream of vRNP nuclear import and viral mRNA synthesis.

KIF13A depletion favors transport of vRNP but not that of HA and M2

Given that KIF13A had been shown to bind and transport Rab11 vesicles (Delevoye et al., 2014), and vRNPs had been shown to use Rab11 vesicles in order to reach sites of assembly (Amorim et al., 2011; Avilov et al., 2012; Eisfeld et al., 2011; Momose et al., 2011), we sought to observe the effect of KIF13A-depletion regarding vRNP localization during the course of infection. It is well established that, at early time points, vRNPs accumulate in the nucleus (where they are synthesized) and from 6 h onwards localize mainly in the cytoplasm. Cytosolic vRNPs start to accumulate at the microtubule organizing center (MTOC) and then become dispersed throughout the cytosol, colocalizing with the host protein Rab11 in puncta that enlarge over time (Amorim et al., 2011). Enlarged puncta were shown to correspond to clustered vesicles that result from impaired vesicular flow (Vale-Costa et al., 2016; Vale-Costa and Amorim, 2016a). The nuclear and/or cytoplasmic time-dependent changes in vRNP localization as assessed by NP staining (Fig. 2A,B) and Pearson correlation values (Fig. 2C) between vRNPs and Rab11 were not statistically different in cells treated with KIF13A and non-targeting siRNAs. This indicates that, in the absence of KIF13A, vRNPs still colocalize with Rab11, and suggests that the lack of this molecular motor does not interfere with the loading of progeny RNA into recycling membranes. However, accumulation of vRNPs at the periphery was significantly less in KIF13A-depleted cells (Fig. 2E). Thus, we concluded that KIF13A is required for the peripheral positioning of vRNPs. Interestingly, the previously reported progressive enlargement in Rab11 and vRNPs cytoplasmic areas (Amorim et al., 2011; Chou et al., 2013; Eisfeld et al., 2011; Lakdawala et al., 2014; Vale-Costa et al., 2016) was reduced relative to the control (Fig. 2D), suggesting either a decrease in vesicular biogenesis or in movement (Delevoye et al., 2014) in the absence of KIF13A.

We also asked whether KIF13A interfered with the levels of the viral transmembrane proteins HA and M2 that are delivered to the surface by a Rab11-independent membrane trafficking pathway (Doms et al., 1993). Cells were treated with control and KIF13A-specific siRNAs, and challenged with PR8. At 10 hpi the surface levels of HA and M2 were measured by flow cytometry. KIF13A-depleted cells presented higher amounts (∼150% and ∼130%, respectively) of these two viral proteins at the surface when compared to control cells (Fig. 2F). As previously proposed (Amorim et al., 2013), this result suggests that HA and M2 proteins are transported to the cell surface normally, but are not released because of reduced viral egress, i.e. reduced release of virus from the host cell.

Our data strongly indicate that KIF13A influences the transport of vRNPs on Rab11 vesicles without interfering with the trafficking of other viral transmembrane proteins.

KIF13A overexpression influences distribution of vRNP to the cell periphery

Our data indicate that KIF13A impacts on the cytoplasmic distribution of vRNPs. To further verify this observation, cells were transfected

Journal of Cell Science (2017) 130, 4038-4050 doi:10.1242/jcs.210807

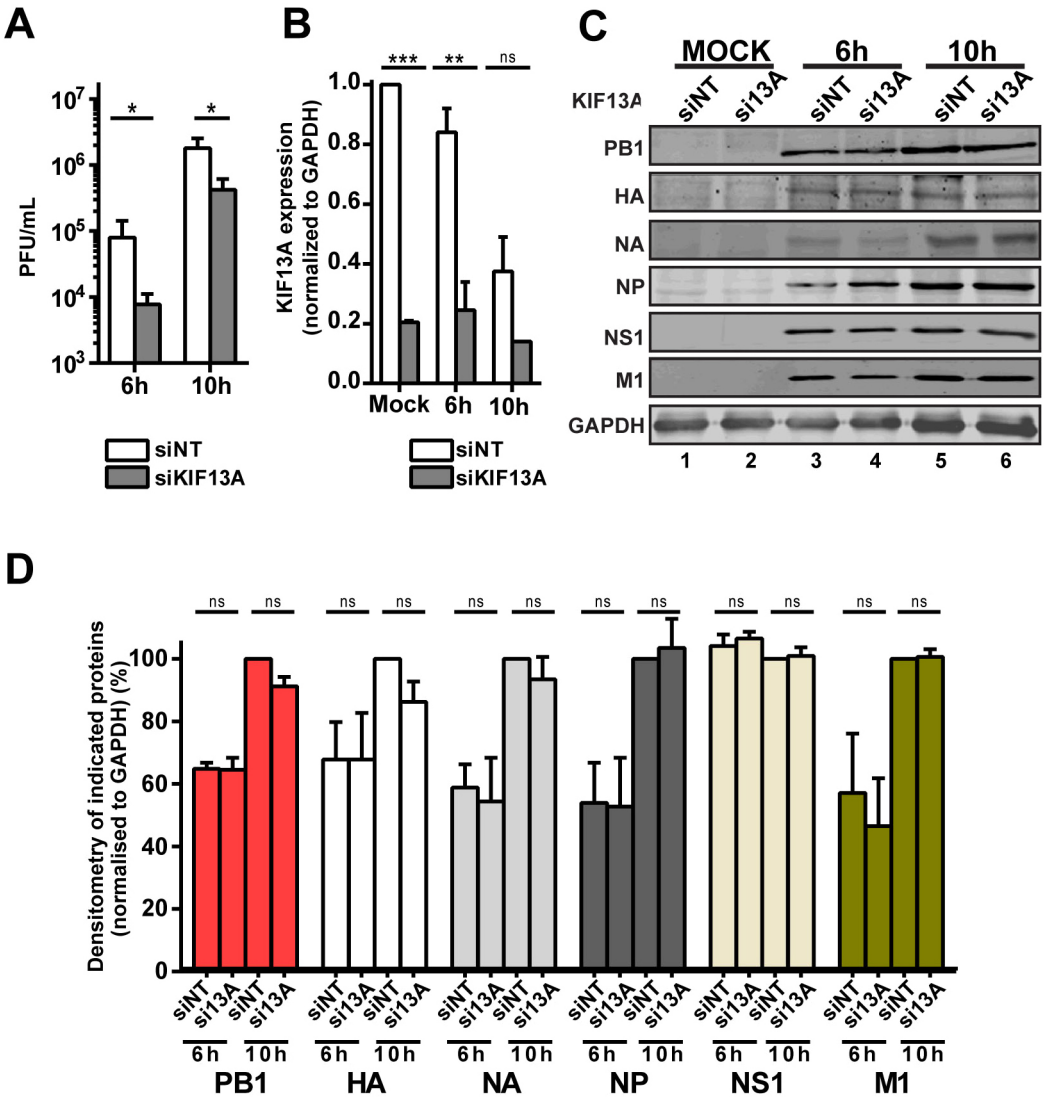

Fig. 1. KIF13A depletion leads to a drop in virus titers, without affecting viral protein expression. A549 cells were treated with non-targeting or KIF13A-specific siRNAs and infected or mock-infected with PR8 at a multiplicity of infection (MOI) of 3. (A) At the indicated time points, supernatants were collected and viral production was evaluated in plaque assays by using MDCK cells. Statistical analysis of data was performed using non-parametric Kolmogorov–Smirnov test, unpaired (*P<0.05). (B) KIF13A expression was evaluated at the level of transcription by RT-qPCR in relation to GAPDH. (C) Viral protein expression of PB1, HA, NA, NP, NS1, M1 and the control GAPDH analysed by western blotting. (D) Expression of viral proteins was quantified and normalized to GAPDH and presented as the percentage of each protein in the non-targeting siRNA condition at 10 h. Data are shown as means±s.e.m. from four independent experiments and statistical significance is indicated as **P<0.01, ***P<0.001 by non-parametric two-way ANOVA tests followed by Tukey multiple comparison test.

with GFP as control, or with either GFP-KIF13A-WT or a GFP-tagged truncated form of KIF13A (GFP-KIF13A-ST) (see Fig. 3D) that is able to attach vesicles but not microtubules (previously described by Delevoye et al., 2014). Cells were subsequently infected or mock-infected with PR8, and NP distribution was assessed during infection. In mock-infected cells, the three proteins distributed as described before (Delevoye et al., 2014). GFP dispersed throughout the cytosol (Fig. 3A; Figs S2A and S3). KIF13A-WT was found in the cytosol (in tubules and puncta), accumulating in peripheral spots (Fig. 3B; Figs S2B and S3B), partially colocalizing with Rab11 (Fig. 3B). KIF13A-ST localized to cytosolic puncta also occupied by Rab11 (Fig. 3C; Figs S2C and S3C). In infected cells transfected with GFP, NP displayed similar time-dependent changes in localization to those described above (Amorim et al., 2011, 2013; Vale-Costa and Amorim, 2016a), i.e. early nuclear accumulation, followed by cytoplasmic display from 6 h onwards. The cytoplasmic phase of vRNPs included the initial accumulation of vRNA in discrete puncta (and perinuclar accumulation) and, at later time points, the discrete puncta were replaced by larger structures dispersed throughout the cytoplasm (Fig. 3A; Figs S2A and S4A). Overexpression of KIF13A-WT resulted in extensive tubulation of the membrane associated with vRNPs, in close proximity to KIF13A tracks (Fig. 3B). Further, it led to the accumulation of vRNPs at the periphery in areas containing Rab11 agglomerates and KIF13A [Fig. 3B; Figs S2B and S4B, (untreated)]. To understand whether KIF13A-dependent vRNP peripheral localization required its motor activity, the distribution of NP was assessed in cells expressing GFP-KIF13A-ST. Strikingly, NP localization was similar to that observed with the GFP control and, at 8 and 10 hpi, GFP-KIF13A-ST was found juxtaposed (partially colocalizing with) to vRNP-Rab11 enlarged puncta [Fig. 3C; Figs S2C,D and S4C (untreated)]. To measure the vRNP peripheral accumulation under the different conditions over the course of

Journal of Cell Science (2017) 130, 4038-4050 doi:10.1242/jcs.210807

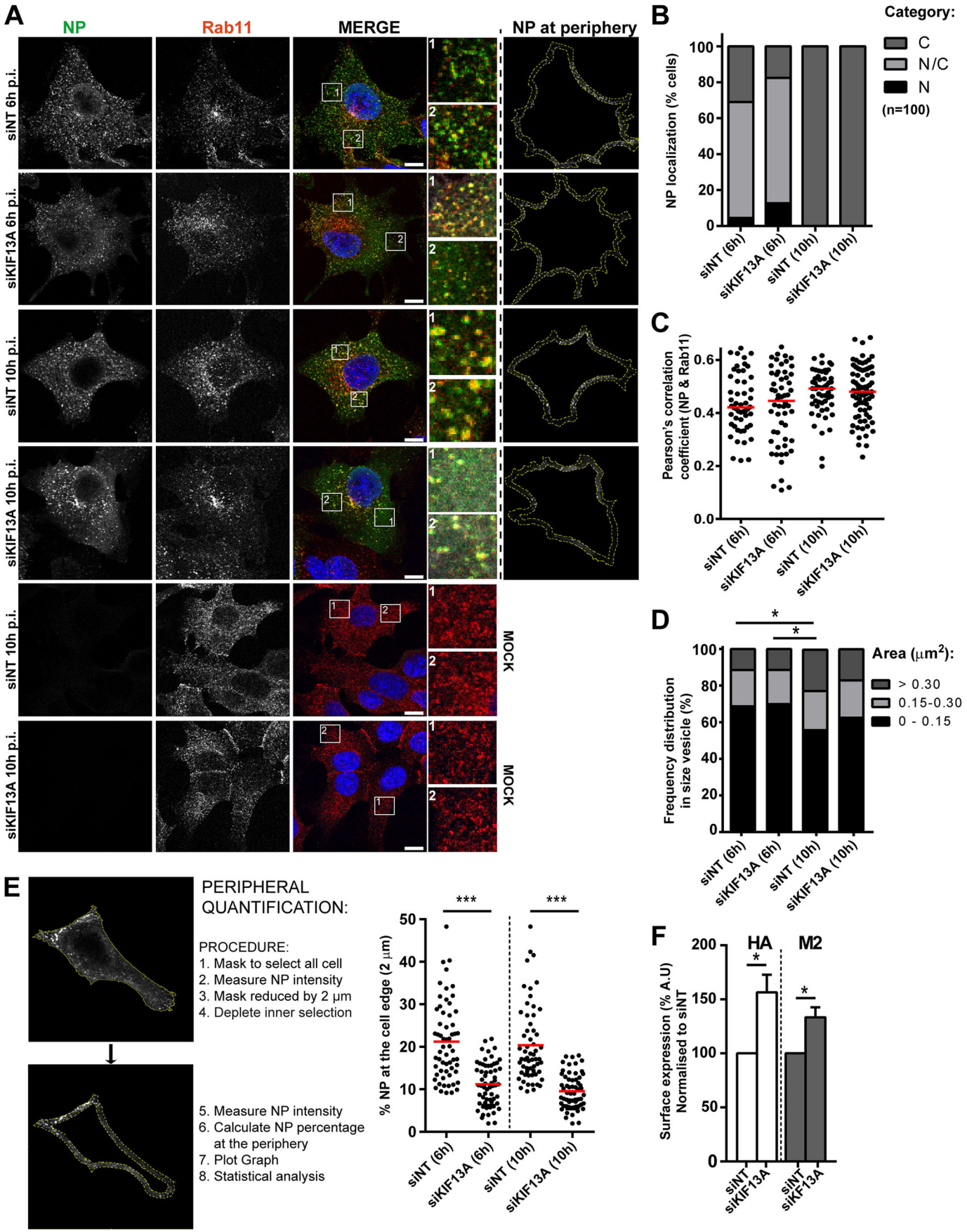

Fig. 2. See next page for legend.

Journal of Cell Science (2017) 130, 4038-4050 doi:10.1242/jcs.210807

Fig. 2. KIF13A depletion reduces the levels of vRNPs close to the plasma membrane, but not that of the viral transmembrane HA and M2 proteins. A549 cells were treated with non-targeting or KIF13A-specific siRNAs and infected or mock-infected with PR8 at an MOI of 3. At indicated time points, cells were fixed and processed for immunofluorescence staining of endogenous Rab11 (red) and viral NP protein (as proxy for vRNPs and in green). (A) Images were acquired by using an SP5 confocal microscope (scale bars: 10 µm). Panels on the right show NP staining (black and white) within 2 µm from the cell edge that was obtained as demonstrated for panel E. Boxed areas in merge panels labeled 'merge' are shown at 3.5x magnification to the right of these panels. (B) 100 cells per condition were evaluated and quantified for nuclear (N), nuclear-cytoplasmic (N/C) or cytoplasmic (C) localization of NP. Statistical analysis was performed using two-way ANOVA followed by Sidak's multiple comparison test and no differences were found. (C) Pearson correlation for NP and Rab11 was calculated at least on 50 cells per condition in three independent replicates using the Fiji plugin colocalization threshold. Statistical analysis was performed using one-way ANOVA followed by Kruskal–Wallis multiple comparison test and and no differences were found. (D) The frequency distribution of three size categories in the areas (in μm^2) of Rab11-vesicles (small, medium and large) was calculated on the basis of NP staining, and plotted. Statistical analysis of data was performed using an ANOVA test and were considered significant at $^*P<0.05$. Per condition, 30 cells were analyzed in four independent experiments. Statistical analysis herein indicated compares only the larger interval of all samples of the four replicates. (E) The amount of NP (in percent) at the edge of the cell was quantified by calculating the ratio of NP intensity within 2 µm from the plasma membrane to NP intensity of the whole cell. The value of 30 cells in three replicates was plotted and analysed statistically by using one-way ANOVA followed by Tukey's multiple comparisons test and were considered significant at $^{***}P<0.001$. (F) A549 cells were treated with non-targeting or KIF13A-specific siRNAs and infected or mock-infected with PR8 at an MOI of 3. At 10 hpi, the surface levels of viral HA and M2 proteins (in percent) were analysed by flow cytometry and plotted as % arbitrary units (A.U.). Statistical analysis was done using one-way ANOVA followed by the Sidak method to compare samples for three replicates, and were considered significant at $^*P<0.05$.

infection, we applied the same method as that described in Fig. 2E. NP peripheral localization (relatively to the whole cell) in cells challenged with PR8 and transfected with either GFP or GFP-KIF13A-ST did not differ during the course of infection. However, NP peripheral localization in cells transfected with GFP-KIF13A-WT was significantly higher (P value <0.01 or <0.001) than under other conditions at the times tested. Our results, therefore, show that KIF13A can influence the distribution of vRNP-containing-Rab11 vesicles by using its motor activity.

KIF13A has been shown to interact with the three isoforms of Rab11 (Rab11a, Rab11b and Rab25) in yeast two-hybrid systems and pull-down assays (Nakagawa et al., 2000; Delevoye et al., 2009, 2014). Rab11a and Rab11b are highly similar and are both implicated in IAV infection (Bruce et al., 2010). Attempts to observe a vRNP-Rab11–KIF13A complex at endogenous levels failed. In cells overexpressing GFP, GFP-KIF13A-WT or GFP-KIF13A-ST together with either Cherry-Rab11a WT or Cherry-Rab11b WT, Rab11a and Rab11b were selectively pulled down with both forms of KIF13A in mock-infected and infected cells at very low but similar levels (Fig. 4). This result suggests that infection does not change this interaction, which is in contrast to what has been described for FIPs (Vale-Costa et al., 2016). However, the low levels of Rab11a and/or Rab11b selectively purified with KIF13A were insufficient to specifically pull down vRNPs (Fig. 4), and whether vRNPs form a tripartite complex together with Rab11 and KIF13A remains to be explored.

vRNP agglomeration induced by the drug nucleozin is affected by KIF13A overexpression

Given that we found no biochemical association between KIF13A, Rab11 and RNPs, we sought to confirm if KIF13A impacts the vRNP distribution in IAV-infected cells by using several additional complementary strategies. First, we used the drug nucleozin (Kao et al., 2010), which has previously been demonstrated to permanently bind colliding vRNP-Rab11-vesicles when added at late time points (Amorim et al., 2013). Briefly, the drug was shown to have affinity for several domains on NP (the viral protein coating vRNPs) (Kao et al., 2010) and, hence, when vesicles (carrying vRNPs on the outside) collide, they attach to each other. As time progresses, nucleozin-induced vRNP-Rab11 vesicular agglomerates increase in size, producing dramatic structures that collapse near the MTOC (for detailed description on nucleozin see Kao et al., 2010; Amorim et al., 2013). Of note, as nucleozin has an affinity for NP and not Rab11, its action is specific to infected cells (compare treated and untreated samples in Figs S3 and S4, and see Amorim et al., 2013). In contrast to the nucleozin induced movement of vRNPs to the perinuclear region, KIF13A transports Rab11 vesicles towards the cell surface (Delevoye et al., 2014). Hence, we reasoned that KIF13A counteracs the action of nucleozin by applying a force in the opposite direction that would alter either (a) the shape of agglomerated vesicles or (b) the time agglomerates take to collapse at the perinuclear region (Fig. 5C).

Consistent with exerting opposing forces, nucleozin-treated cells overexpressing GFP-KIF13A-WT show vRNP-agglomerates more distant from the nucleus than those observed in cells expressing GFP (as control) or GFP-KIF13A-ST (without motor capacity) (Fig. 5A). For an unbiased and accurate quantification of nucleozin-induced perinuclear accumulation of vRNPs and/or Rab11, we generated an automated tool to evaluate the amount of vRNPs/Rab11 within 2 µm from the nucleus (Fig. 5B). Staining of both NP and Rab11 was significantly less intense close to the nucleus in cells overexpressing GFP-KIF13A-WT and treated with nucleozin when compared to that in cells with GFP or GFP-KIF13A-ST, indicating that KIF13A operates as a force able to counteract the action of nucleozin (Fig. 5B).

Nucleozin-induced vRNP-agglomerates were shown to include Rab11 (Amorim et al., 2013; and Fig. 5D, right) but exclude a series of organelle markers (Golgi, endoplasmic reticulum, lysosomes). We reasoned that, given that the candidate proteins exhibit similar dynamics of vRNP colocalization and are specifically trapped in nucleozin-induced vRNP aggregates, they form functional complexes with the vRNPs (Amorim et al., 2013). To understand whether this was the case for KIF13A, we quantified Pearson correlation values of GFP, GFP-KIF13A-WT, GFP-KIF13A-ST with vRNPs and Rab11. GFP and GFP-KIF13A-WT were found not to colocalize with vRNPs or Rab11 in infected cells, regardless of nucleozin. However, as just demonstrated, GFP-KIF13A-WT counteracts nucleozin-induced aggregate formation by exerting a force in the opposite direction and, with GFP fused to the motor part, proximity between all components could be hard to evaluate in this system. Hence, we reasoned that GFP-KIF13A-ST is a better choice for this measurement, as it lacks the pulling capacity. In agreement, in the presence of nucleozin, GFP-KIF13A-ST colocalized with both vRNPs and Rab11, consistent with being in close proximity to both (Fig. 5D). Together, our results suggest that KIF13A not only influences the location of vRNPs and Rab11 in infected cells, but is also part of a complex with these vesicles.

KIF13A favors distribution of mitoRab11-vRNP to the surface

As a second additional strategy, in order to understand whether KIF13A transports vRNPs on Rab11 vesicles and as a way to discriminate whether it binds to either Rab11a or Rab11b, we used an artificial targeting system to anchor Rab11a and Rab11b to the

Journal of Cell Science

Journal of Cell Science (2017) 130, 4038-4050 doi:10.1242/jcs.210807

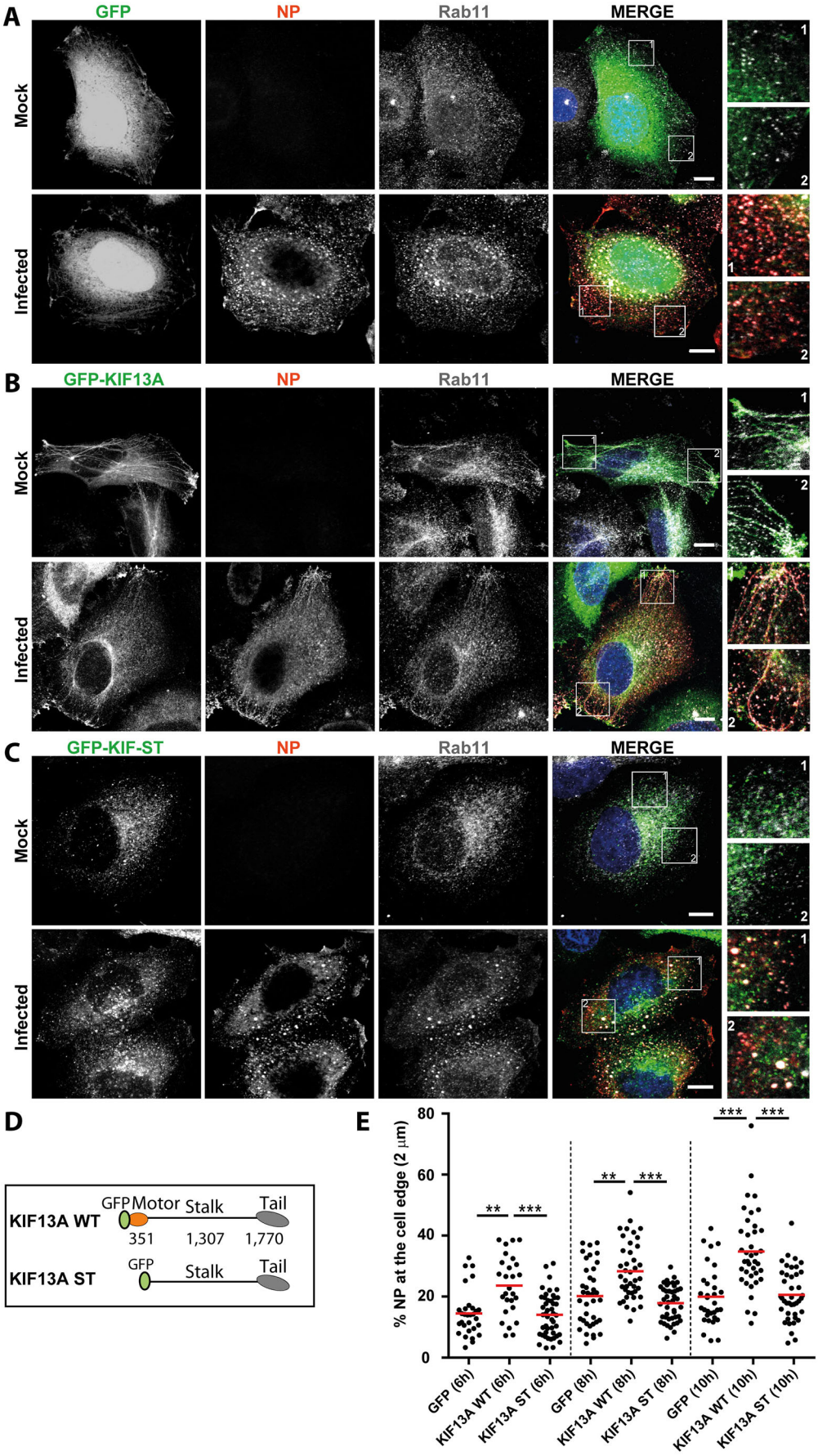

Fig. 3. KIF13A overexpression favors NP distribution to the cell edge and requires KIF13A binding to microtubules. (A-C) HeLa cells were transfected with GFP (A) GFP-KIF13A-WT (GFP-KIF13A) (B) or GFP-KIF13A-ST (GFP-KIF-ST) (C). At 24 h post transfection cells were infected (or mock-infected) with PR8 at an MOI=3. After 8 hpi cells were fixed and stained for NP (red), endogenous Rab11 (gray) and counterstained with DAPI (scale bars: 10 μm). Boxed areas highlight the proximity between KIF13A and vRNP-Rab11 vesicles and are magnified to the right of these panels. (D) Sketch of KIF13A wild-type (WT) and mutant (KIF13A-ST) forms. (E) The amount of NP at the edge of the cell was quantified in percent by calculating the ratio of NP intensity within 2 μm from the plasma membrane to the NP intensity of the whole cell. Data obtained of 25 cells and three replicates were plotted and analysed statistically by using one-way ANOVA followed by Tukey's multiple comparisons, and were considered significant at $^{**}P<0.01$ and $^{***}P<0.001$.

Journal of Cell Science (2017) 130, 4038-4050 doi:10.1242/jcs.210807

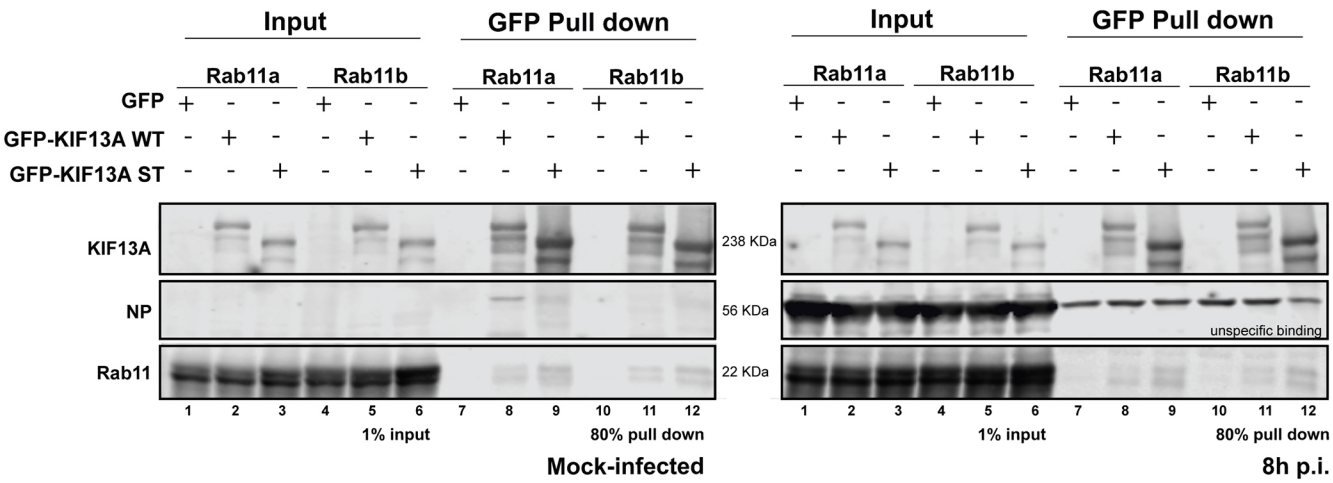

Fig. 4. GFP-KIF13A-WT and GFP-KIF13A-ST pull down Rab11a and Rab11b. HEK293T cells were transfected individually as indicated with GFP, GFP-KIF13A-WT or GFP-KIF13A-ST in combination with either Cherry-Rab11a-WT or Cherry-Rab11b-WT. 24 h post-transfection cells were infected (or mock-infected) with PR8 at an MOI=3 and at 8 hpi, GFP was immunoprecipitated by using GFP-TRAP. Input (1% of total) and pulled down complexes (80% of total) were separated by electrophoresis, and KIF13A, NP and Rab11 analysed by western blotting. The western blot is representative of three independent experiments.

mitochondria (by fusing constitutively active (CA) Rab11a/b to the mitochondrial targeting sequence (MTS) of Tom20 (henceforward referred to as mitoRab11a/b) and analyse relocation of individual effectors (Fig. 6B). This strategy has been successfully used by us to show that FIPs competed with vRNPs for Rab11a binding (Vale-Costa et al., 2016). Constitutively active mitoRab11a but not mitoCherry control recruited FIPs to the mitochondria (Vale-Costa et al., 2016) (Fig. S5A). When vRNPs and FIPs were coexpressed, a decrease in vRNP localization to the mitochondria was observed (Vale-Costa et al., 2016). We applied the same protocol here and transfected mitoCherry or mitoRab11a/b and GFP or GFP-KIF13A-WT or GFP-KIF13A-ST before infecting and mock infecting cells. In mock or infected cells, GFP and GFP-KIF13A-WT did not relocalize to mitochondria (Fig. 6; Figs S5B,C and S6). However, GFP-KIF13A-ST, in the presence of mitoRab11a but not mitoCherry, was found juxtaposed to this organelle (Fig. 6; Figs S5B,C and S6), indicating that, if not part of the complex, this motor (when not exerting pulling forces) is found in close proximity to mitoRab11a. During infection, vRNPs redistributed to the mitochondria in an undifferentiated manner regardless of KIF13A (Fig. S5 and Fig. 6A-C). Furthermore, overexpression of GFP-KIF13A-WT favors the distribution of mitoRab11a (Fig. 6A,C; Fig. S5B,C middle panels, Fig. S6) and of vRNPs to places at the cell surface displaying GFP-KIF13A-WT (Fig. 6; Fig. S5C). Similar observations were acquired for mitoRab11b. Quantification of peripheral localization of mitoRab11a or mitoRab11b, and of vRNPs was done by measuring the percentage of these components within 3 µm of the plasma membrane relative to the whole cell (3 µm were chosen given the large size of mitochondria). In the presence of GFP-KIF13A-WT, mitoRab11a/b and vRNPs were found significantly closer to the periphery than the control GFP, confirming the results obtained. In addition, this favored localization was, at least for mitoRab11b and vRNPs, dependent of the motor activity of KIF13A, as the truncated form of KIF13A failed to do so to the same extent (Fig. 6C,D; Figs S5 and S6).

DISCUSSION

It had previously been shown that vRNPs are transported to the cell periphery using the recycling pathway (via Rab11) at speeds compatible with movement along microtubules (Amorim et al., 2011; Avilov et al., 2012; Eisfeld et al., 2011; Momose et al., 2011). In addition, it is well established that IAV not only uses the recycling pathway but alters it – as demonstrated by Rab11 re-distribution during infection – changing from distinct puncta to enlarged structures (Lakdawala et al., 2014; Chou et al., 2013; Amorim et al., 2011; Avilov et al., 2012; Eisfeld et al., 2011). Mechanistically, Rab11 alterations were reported to be, at least partially, a consequence of a virus-induced halt in recycling endosome functioning (Vale-Costa et al., 2016; Vale-Costa and Amorim, 2016a). Several lines of evidence support this hypothesis, including the findings that transferrin recycling upon infection is reduced (Kawaguchi et al., 2015; Vale-Costa et al., 2016) and the recruitment of bona fide Rab11 effectors decreases, as well as the demonstration that Rab11 enlarged puncta are composed of clustered vesicles (Vale-Costa et al., 2016; Vale-Costa and Amorim, 2016a) that contain the pool of the eight vRNPs (Chou et al., 2013; Lakdawala et al., 2014). Whether vesicular clustering serves a function has not been determined. One appealing hypothesis is that these sites serve to concentrate vRNPs and promote viral genome assembly. Such hypothesis is in contrast to other recently proposed models suggesting that genome assembly occurs gradually when ERC vesicles collide on route to the plasma membrane, with the sequential formation of vRNP sub-bundles (containing less than eight vRNPs) as reviewed by Lakdawala et al., 2016. The latter model is supported by an increase in colocalization of the eight segments found in the Rab11 enlarged structures (rather than distinct dots) induced by viral infection. Approaches able to resolve whether in clustered vesicles (or Rab11 enlarged structures), the eight segments are found in a complex are necessary to validate one of the models.

IAV modulation of the recycling pathway (Rab11 vesicles) and, in particular, competition between vRNPs and FIPs for Rab11 binding, raised the important question of which host factors – with special attention to molecular motors – are involved in carrying vRNP-laden Rab11 vesicles to the cell periphery (Amorim et al., 2011; Eisfeld et al., 2011; Avilov et al., 2012; Momose et al., 2011). Here, we have identified the first motor protein able to do so. Lack of KIF13A was found to reduce viral titers (Fig. 1A), without affecting initial stages of viral infection (Fig. 1C,D) or the delivery of virion-forming viral proteins (HA and M2) (Fig. 2F) to sites of virus assembly but impacting on vRNP localization. In the context of overexpression,

Journal of Cell Science (2017) 130, 4038-4050 doi:10.1242/jcs.210807

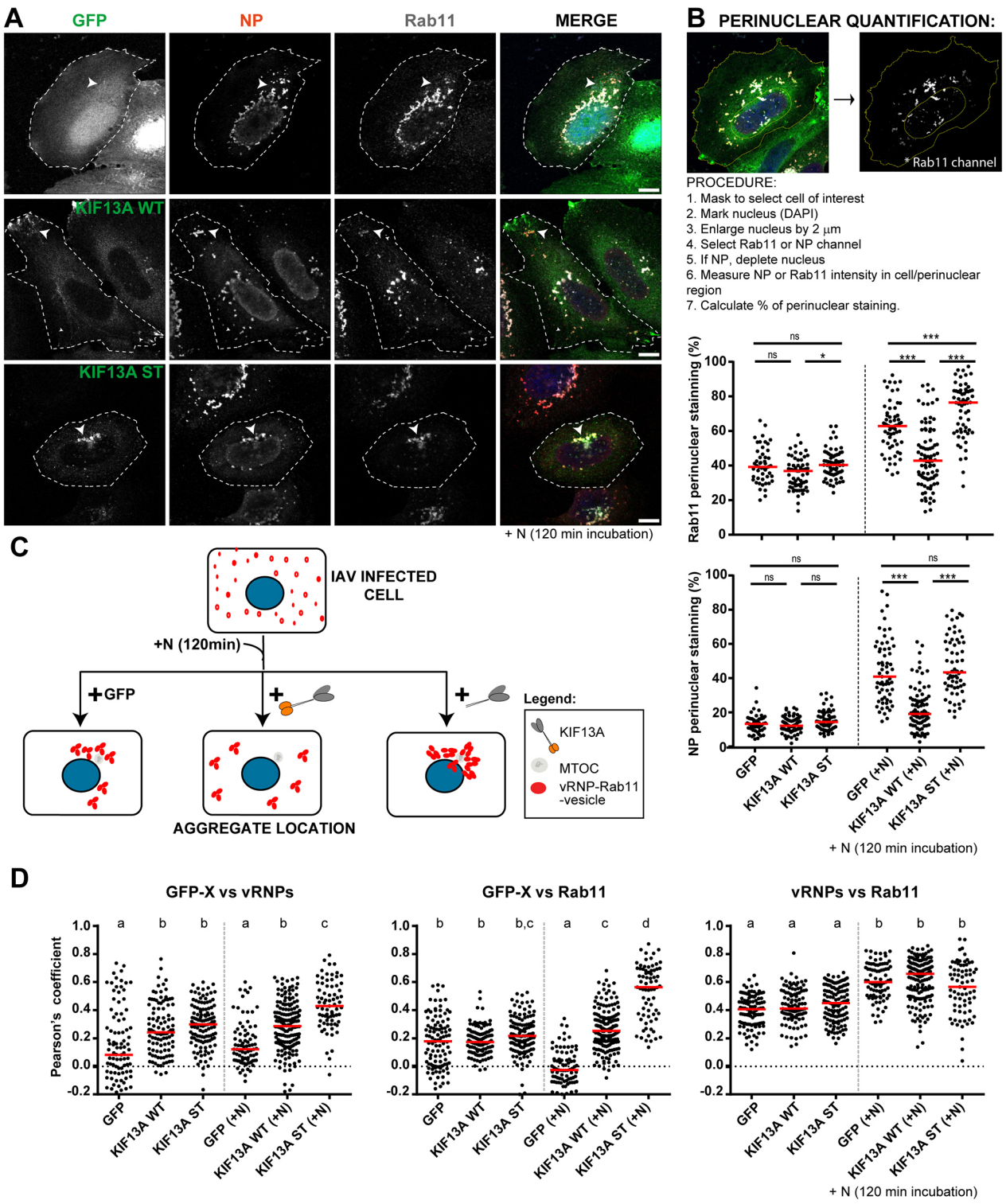

Fig. 5. See next page for legend.

KIF13A favored the distribution of vRNPs and Rab11 towards the periphery under three different conditions: normal infection (Fig. 3; Figs S2, S3 and S4), upon treatment with nucleozin (Fig. 5; Figs S3 and S4) and when Rab11 was artificially tagged to the mitochondria (Fig. 6; Figs S5 and S6). Immunoprecipitation experiments of GFP-KIF13A-WT, selectively retrieved Rab11a and Rab11b, albeit at low levels, which might justify the failure to show vRNP associated to the complex (Fig. 4). This association between Rab11 and KIF13A was further corroborated by our strategies using nucleozin and mitoRab11a and/or Rab11b that placed all the components in close proximity at the plasma membrane (Figs 5, 6; Figs S2-S6). Together, these results support the model shown in Fig. 7, in which, in contrast to what was observed for FIPs – and, presumably, the molecular motors these attract – KIF13A binding to Rab11 vesicles is not disrupted by infection and facilitates vRNP transport to the periphery.

Journal of Cell Science (2017) 130, 4038-4050 doi:10.1242/jcs.210807

Fig. 5. Nucleozin-induced collapse of vRNP aggregates close to the nucleus is less pronounced in the presence of KIF13A. HeLa cells were transfected individually with GFP, GFP-KIF13A-WT (KIF13A WT) or GFP-KIF13A-ST (KIF13A ST); 24 h post transfection cells were infected (or mock-infected) with PR8 at an MOI=3, and at 8 hpi 2 µM nucleozin was added and incubated for 2 h. Cells were then fixed and stained for NP (red) and Rab11 (gray), and counterstained with DAPI. (A) Representative images of three independent experiments (scale bars: 10 µm). Dashed lines encircle cells that had been transfected with indicated plasmids and were infected; arrowheads indicate the location of vRNPs-Rab11 complexes. (B) The amount of vRNPs (by measuring NP) and Rab11 close to the nucleus (within 2 µm) relative to that found in the whole cell was quantified (in percent) in 60 cells and plotted. Data obtained from 20 cells in three replicates were plotted and analysed statistically by using two-way ANOVA followed by Tukey's multiple comparisons test and considered not significant (NS) or significant at $*P<0.05$ and $***P<0.001$. (C) Model explaining how KIF13-WT counteracts the action of nucleozin. It has been reported that nucleozin [(+N 120 min)] has the affinity for three binding sites on NP and, hence, crosslinks colliding vRNP-laden Rab11 vesicles, resulting in large agglomerates that collapse near the nucleus. In our experimental set up, addition of GFP (+GFP, left) did not affect the collapse of vRNPs-Rab11 vesicles, but that of GFP-KIF13A-WT (middle) resulted in decreased perinuclear levels of vRNPs, suggesting that KIF13A counteracts nucleozin action by pulling vRNPs away from the MTOC. KIF13A action required binding to microtubules, as the mutant KIF13A-ST (right) was unable to counteract nucleozin action. (D) Pearson correlation values between GFP-X (X= KIF13A-WT or KIF13A-ST) and vRNPs or Rab11, as well as between vRNPs and Rab11 in the presence and absence of nucleozin were calculated for at least 50 cells per condition and three independent replicates, by using the Fiji plugin colocalization threshold. Statistical analysis was performed using one-way ANOVA followed by Kruskal–Wallis multiple comparison test; letters a, b, C and D indicate comparisons that are significant at least $P<0.01$.

The accumulating data regarding alterations in the Rab11 pathway led to the proposal that, during IAV infection, Rab11 is not the final factor delivering vRNPs to the surface, handing vRNPs to an additional host protein(s) prior to reaching the membrane (the Rab11 'way-station' hypothesis) (Eisfeld et al., 2015; Vale-Costa et al., 2016; Vale-Costa and Amorim, 2016a). In agreement, a very recent paper provides evidence of a step during the cytoplasmic transport of influenza vRNPs that is independent of Rab11a (Nturibi et al., 2017). Our results show GFP-KIF13A-WT accumulating at the plasma membrane (Figs 3, 5, 6; Figs S2-S6) juxtaposed to vRNPs and Rab11, supporting the notion that KIF13A operates in a Rab11-dependent manner. However, the way-station hypothesis might not be discarded, as vRNPs might be transferred from Rab11 to other cellular factor(s) and might slide to the cell surface mediated by molecular motors distinct from KIF13A.

It has been shown that impairment of Rab11 vesicular flow leads to clustering of vesicles (Vale-Costa et al., 2016), but the step(s) affected are not fully understood. Here, we focused on vesicular transport on microtubules without investigating other steps required for the vesicular flow (i.e. biogenesis, attachment and fusion); the latter three also lack characterization. It is clear that KIF13A does not prevent vesicular clustering at late stage of IAV infection, although it contributes to deliver vRNP-laden Rab11 vesicles to the surface. Whether KIF13A contributes to vesicular clustering requires further investigation. One attractive hypothesis is that, at late stages of infection, the virus reduces the level of KIF13A (Fig. 1B), thus aggravating the impairment in vesicular transport. Other mechanisms might contribute to halt the Rab11 pathway during IAV infection. Alterations of the cytoskeletal structure have been reported to create obstacles to vesicular transport, leading to pausing and inhibition of movement (Gramlich et al., 2017; Verdeny-Vilanova et al., 2017). IAV has been shown to alter the structure of microtubules, and of their associated proteins and enzymes, resulting, for example, in enhanced microtubule acetylation, a modification shown to affect microtubule-based movement (Badding and Dean, 2013). However, these alterations in vRNP transport have not been analyzed (Husain and Harrod, 2011). Another parameter worth investigating is how the loading of heavy and large vRNPs influences vesicular transport (Verdeny-Vilanova et al., 2017). Seminal studies imaged fully assembled IAV genomes that were budding at the plasma membrane (Fournier et al., 2012; Sugita et al., 2013). However, the precise cellular location where genome assembly takes place remains unclear. Recent findings suggested that genome assembly involves formation of vRNP sub-bundles (Chou et al., 2013; Lakdawala et al., 2014). Formation of sub-bundles could lead, or at least contribute, to a halt in vesicular movement resulting in clustering of Rab11 vesicles. Whether clustering of Rab11 vesicles triggers genome assembly or results from partial genome assembly – creating an environment that is able to facilitate its completion – is still unclear (Vale-Costa et al., 2016; Vale-Costa and Amorim, 2016a). Intriguingly, studies that employed high-resolution electron microscopy found no clear evidence of supramolecular complexes in the areas of clustered vesicles (Vale-Costa et al., 2016), although it is very unlikely that the resolution required for such claim has been attained. All these studies highlight the fact that the assembly of the IAV genome is far from understood. Fascinating outstanding questions that await clarification include: (1) Do vRNPs reach the budding sites at the plasma membrane as a sort of supramolecular complex (sub-bundle or complete genome)? (2) Does vesicular clustering contribute to viral assembly? (3) What are the molecular mechanisms that lead to vesicular clustering? (4) Is Rab11 the final carrier of vRNP-containing vesicles to the plasma membrane? And, finally, (5) what other means does the virus explore in order to transport vRNPs (and other viral proteins) to assembly sites?

MATERIALS AND METHODS

Cells, viruses, plaque assays, infections and drugs

Human epithelial embryonic kidney (HEK293T) (gift from Dr Colin Adrain, IGC, Portugal), cervical HeLa and alveolar basal cells (A549), and Madin-Darby canine kidney cells (MDCK), used to titrate the virus, were cultured as described before (Amorim et al., 2011). Cell lines were a kind gift from Prof Paul Digard (Roslin Institute, Edinburgh, UK). All cells are regularly tested for mycoplasma contamination. Reverse-genetics-derived A/Puerto Rico/8/34 (PR8) was used as a model virus (de Wit et al., 2004) and titrated according to Matrosovich et al., 2006. Statistical analysis of data was done using non-parametric Kolmogorov–Smirnov tests. Additional statistical analyses included a two-way ANOVA test (to include time), followed by Turkey's or Sidak's multiple comparison test ($*P<0.05$, $**P<0.01$, $***P<0.001$, ns non-significant). Virus infections were performed at an MOI of 3, usually carried out as described previously (Amorim et al., 2011), or MOI=10 for the mitoRab11 experiment (as described by Vale-Costa et al., 2016). After 30 min, cells were overlaid with DMEM containing 0.14% bovine serum albumin. The drug nucleozin (Kao et al., 2010) (gift from Richard Kao, University of Hong Kong, China) dissolved in DMSO was used at a final concentration of 2 µM. Reverse genetic plasmids were contributed by Dr Ron Fouchier (Erasmus University Medical Center, Rotterdam, Netherlands).

Plasmids produced during this study

Plasmids encoding GFP-tagged wild-type KIF13A (GFP-KIF13A-WT) and GFP-tagged truncated KIF13A (GFP-KIF13A-ST) were subcloned into pEGFP-C2 by using SacI and SalI restriction sites and subsequently amplified by using plasmids described in (Delevoye et al., 2014). GFP-KIF13A-WT and GFP-KIF13A-ST were amplified from pKIF13A-YFP (Graça Raposo). Plasmid encoding Cherry-Rab11bWT was produced by PCR-amplification of cDNA from HeLa cells and cloning into EcoRI–BamHI in pCherry-C2 (Clontech). CA MitoCherry-Rab11b plasmid was produced from Cherry-Rab11b. The constitutively active mutation (Q70L)

Journal of Cell Science (2017) 130, 4038-4050 doi:10.1242/jcs.210807

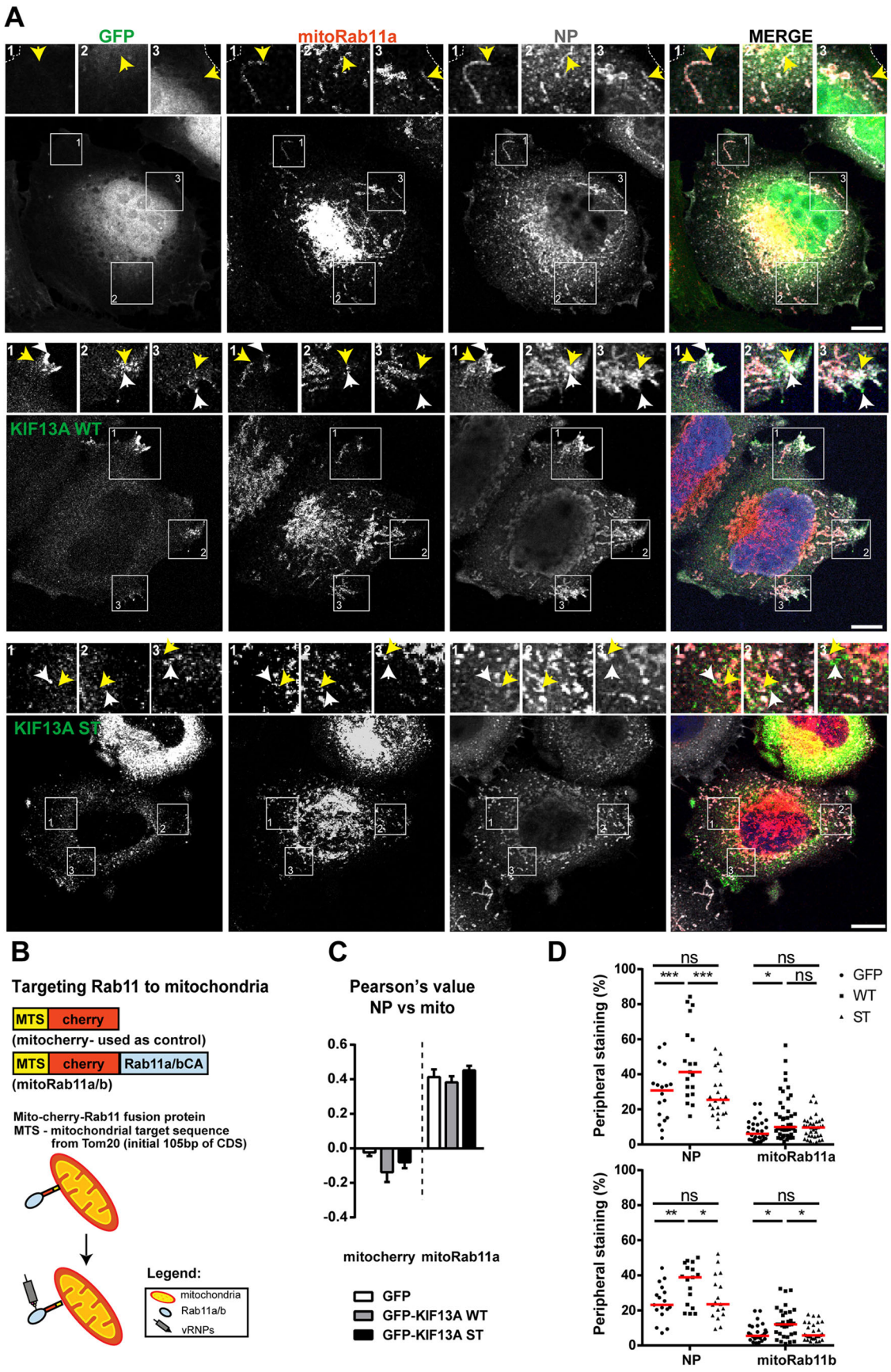

Fig. 6. See next page for legend.

Journal of Cell Science

Journal of Cell Science (2017) 130, 4038-4050 doi:10.1242/jcs.210807

Fig. 6. GFP-KIF13A-WT favors the localization of mitochondria to the periphery when artificially expressing Rab11a or Rab11b. HeLa cells were transfected individually with GFP, GFP-KIF13A-WT (KIF13A WT) or GFP-KIF13A-ST (KIF13A ST) and mitoCherry, mitoRab11a or mitoRab11b. 24 h post-transfection cells were infected (or mock-infected) with PR8 at an MOI=10. At 14 hpi, cells were fixed and stained for NP (gray) and counterstained with DAPI. (A) Representative images of three independent experiments (scale bars: 10 µm). Boxed areas indicate colocalization between vRNPs and Rab11, and the proximity to KIF13A, and are shown at 1.5x to 2.5x magnification above individual panels. White arrowheads indicate GFP-KIF13A-WT or GFP-KIF13A-ST; yellow arrowheads indicate vRNPs and Rab11a. (B) Diagram explaining the strategy used to artificially target Cherry, Rab11a or Rab11b to the mitochondria. (C) Pearson correlation value between NP and mitoCherry, and NP and mitoRab11a were calculated for 20 cells per condition from independent replicates by using the Fiji plugin colocalization threshold. Statistical analysis was performed by using one-way ANOVA followed by Kruskal–Wallis multiple comparison test. (D) The amount of NP and mitoRab11a, and NP and mitoRab11b at the edge of the cell (in percent) was quantified by calculating the ratio of NP intensity within 3 µm from the plasma membrane in relation to the NP: mitoRab11a, and NP:mitoRab11b intensity in the entire cell. Data of at least 20 cells and three replicates were plotted and analyzed statistically using one-way ANOVA followed by Sidak's multiple comparisons test, and considered significant at $*P<0.05$, $**P<0.01$ and $***P<0.001$.

was introduced by site-directed mutagenesis and fused to the first 105 base pairs of the Tom20 MTS cloned upstream of Cherry–Rab11bCA using NheI–AgeI sites.

The following primers were used: GFP-KIF13A-WT Rv: 5′-TCGAGAGCTCAATGTCGGATACCAAGGTAAAAG-3′; GFP-KIF13A-ST Rv: 5′-TCGAGAGCTCAAGGATTGTGAACCATGCTG-3′; GFP-KIF13A-WT and ST Fw: 5′-TCGAGTCGACTCATTGACAGCACAGAAC-3′; Rab11b Rv: 5′-TGCGGATCCTCACAGGTTCTGGCAGCA-3′; Rab11b Fw: 5′-ATGCGAATTCATGGGGACCCGGGAC-3′; mitoRab11b Rv: 5′-ATGCGGATCCTCACAGGTTCTGGCAGCA-3′; mitoRab11b Fw: 5′-ATGCGAATTCATGGGGACCCGGGAC-3′; CA mutation Rv: 5′-GGTAGCGCTCCAGGCCAGCGGTG-3′; CA mutation Fw: 5′-CACCGCTGGCCTGGAGCGCTACC-3′; Tom 20 Rv: 5′-ATGCACCGGTTTGAAGTTGGGGTCACTTCG-3′; Tom 20 Fw: 5′-ATGCGCTAGCATGGTGGGTCGGAACAGC-3′.

Transfections of plasmids and siRNA

Cells (HEK293T or HeLa), grown to 70% confluency in 10-cm dishes were transfected with 250 ng of indicated plasmids using Lipofectamine 2000 (Life Technologies) and Opti-MEM (Life Technologies), according to manufacturer's instructions. Cells were infected or mock infected 24 h post transfection at indicated MOI. siRNA transfection of the KIF13A (5′-CTGGCGGGTAGCGAAAGAGTA-3′, S103019800) and negative control (NT, 1022076) RNA duplexes (QIAGEN) was performed in HEK293T and A549 cells grown to ∼50% confluency the day before transfection. Cells were transfected in 6-well plates (100 pmol/well) using DharmaFECT (Dharmacon). When needed 36 h later, cells were transfected as above. The mitoRab11a/b experiments were done as described by Vale-Costa et al. (2016), except that plasmids transfected together with mitoRab11 or mitoCherry included GFP, GFP-KIF13A-WT or GFP-KIF13A-ST.

Real-time reverse-transcription PCR

Extraction of RNA from samples in NZYol (NZYtech, MB18501) was achieved by using the Direct-zol RNA minipreps (Zymo Research, R2052). Reverse transcription (RT) was performed using the transcriptor first strand cDNA kit (Roche, 04896866001). Real-time RT-PCR to detect GAPDH and KIF13A was prepared in 384-well, white, thin walled plates (Biorad, HSP3805) by using SYBR Green Supermix (Biorad, 172-5124), 10% (v/v) of cDNA and 0.4 µM of each primer (KIF13A Fw: 5′-GAAGGGAATCAAACGGTCCT-3′; KIF13A Rv: 5′-AAACCACTTCTTGACCAGCG-3′; GAPDH Fw: 5′-CTCTGCTCCTCCTGTTCGAC-3′; GAPDH Rv: 5′-ACCAAATCCGTTGACTCCGAC-3′). The reaction was performed on a CFX 384 Touch Real-Time PCR Detection System machine (Biorad), under the following PCR conditions: Cycle 1 (1 repeat): 95°C for 2 min; Cycle 2 (40 repeats): 95°C for 5 s and 60°C for 30 s; Cycle 3: 95°C for 5 s and melt curve 65°C to 95°C (increment 0.05°C each 5 s). Data were analysed using the CFX manager software (Biorad).

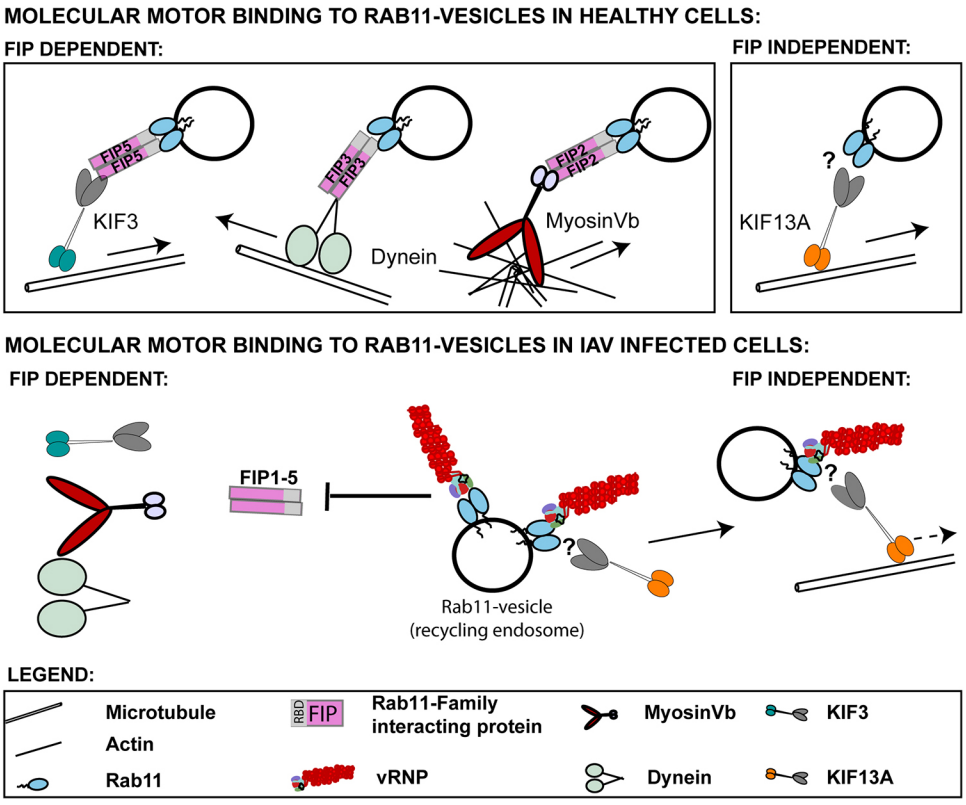

Fig. 7. Model for molecular motor recruitment of Rab11 vesicles during IAV infection. In the healthy cell, GTP-bound Rab11 associates with FIPs that recruit members of the three known types of molecular motor, i.e. kinesin, dynein and myosin. In addition, GTP-Rab11 also attracts molecular motors independently of FIPs, as in the case of KIF13A. We have previously shown that in IAV infected cells, vRNPs outcompete FIPs for Rab11 binding (Vale-Costa et al., 2016). In this study, we report that the molecular motor KIF13A is able to bind and transport vRNP-Rab11 carrying vesicles. At late stages of infection the levels of KIF13A are reduced and might affect transport (indicated by the dashed arrow that implies movement). The exact nature of the molecular players that mediate this interaction in our system is still unclear.

Journal of Cell Science

Confocal microscopy

Immunofluorescence assays were performed as described by Simpson-Holley et al. (2002). Antibodies used were: rabbit polyclonal against Rab11a (1:100; Life Technologies, catalog no. 715300); mouse monoclonal against NP (1:1000; Abcam, catalog no.20343). Secondary antibodies were all from the Alexa Fluor range (1:1000; Life Technologies). Single optical sections were imaged with a Leica SP5 live or inverted confocal microscope and post-processed using ImageJ (National Institutes of Health; NIH) software for analyses. For vesicle-size analysis (area in μm^2), images were converted to 8-bit color and a 'background subtraction' of 20 pixels applied. Subsequently, 'threshold' was adjusted to 14 (lower level) – 255 (upper level), followed by the 'analyze particle' function to quantify each vesicle inside selected cells. Frequency distributions were calculated and plotted by using intervals of [0-0.15], [0.15-0.30] and above 0.30 μm^2; to calculate the Pearson correlation coefficient, the 'Coloc 2' function was used to quantify the amount of NP and Rab11 perinuclear staining (in percent), the perinuclear region was defined by using the nucleus, delineated by DAPI staining that was then enlarged by 2 µm towards the plasma membrane. This 2 µm region was used to measure the intensity of NP (and of Rab11) by using integrated density divided by the integrated density of NP (and Rab11) staining of the entire cytoplasm. The cell membrane was defined by using wheat germ agglutinin (WGA) staining. To quantify accumulation at the periphery the cell edge was defined with WGA, decreased by 2 or 3 µm. The intensity of NP (and of Rab11) was measured within this region by using integrated density and divided by the integrated density of NP (and Rab11) staining of the entire cytoplasm. All graphs were plotted using GraphPad Prism. Statistical analysis of data was performed using two-way ANOVA test, followed by Turkey's or Sidak's multiple comparison test (*P<0.05, **P<0.01, ***P<0.001, ns non-significant). At least 25 cells were analysed per condition.

Flow cytometry

A549 cells were prepared for flow cytometry analysis by detaching from the wells with trypsin, followed by fixation with 4% paraformaldehyde and washing with PBS in between steps. Cell suspensions were then resuspended in FACS buffer (PBS and 4% FBS). Antibodies used for immunofluorescence staining were: rabbit polyclonal against HA (anti-PR8, 1:500, kind gift from Prof Paul Digard) and M2 (1:100, Abcam, catalog no. 56086). Secondary antibodies were from the Alexa Fluor range (1:1000; Life Technologies). Analysis of cell populations was performed in a Becton Dickinson (BD, Franklin Lakes, NJ) FACSCalibur equipped with BD CELLQuest and FlowJo (Tree Star Inc., Ashland, OR) softwares.

Pull-down assays and western blotting

Pull down assays of GFP-bound KIF13A were performed using GFP-tagged magnetic agarose beads (GFP-Trap®_M beads, ChromoTek, gtm-20). HEK293T cells transfected with GFP, GFP-KIF13A-WT or GFP-KIF13A-ST and with Cherry-Rab11a WT or Cherry-Rab11b WT were infected or mock infected at an MOI of 5 24 h post transfection. At indicated times, cells were lysed in 500 µl of the provided lysis buffer containing 1 mM phenylmethylsulfonyl fluoride and protease inhibitor cocktail (Roche) on ice for 30 min. Clarified samples were incubated overnight at 4°C with 20 µl GFP-Trap®_M beads. Pelleted beads were washed extensively with lysis buffer and bound proteins eluted by boiling in SDS-PAGE buffer containing 2.5% β-mercaptoethanol.

Western blotting was performed according to standard procedures and imaged by using a LI-COR Biosciences Odyssey near-infrared platform as described previously (Bruce et al., 2010). Antibodies used included mouse monoclonal against Rab11 (1:500; Abcam, catalog no. 78337) and neuraminidase (7D8, 1:100, gift from Susanna Colaco, Department of Pathology, University of Cambridge, UK); rabbit monoclonal against virus nucleoprotein (1:2000), and polyclonal against PB1, NS1 and HA (all at 1:500) were provided by Prof Paul Digard. Also used were goat polyclonal against GFP (1:2000; Sicgen, catalog no. AB0020) and M1 (1:500, Abcam, catalog no. 20910). The secondary antibodies were from IRDye range (1:10,000; LI-COR Biosciences).

Acknowledgements

The authors acknowledge Prof Paul Digard (Roslin Institute, Edinburgh, UK) for providing reagents (antibodies, cell lines, viral strains and plasmids), and Dr Ron Fouchier (Erasmus University Medical Center, Rotterdam, Netherlands) for the reverse genetics plasmids.

Competing interests

The authors declare no competing or financial interests.

Author contributions

Conceptualization: M.J.A.; Methodology: A.R.-N, F.F., M.A., G.R., C.D., M.J.A.; Validation: F.F., M.A., S.V.-C., M.J.A.; Formal analysis: A.R.-N, M.A., S.V.-C., M.J.A.; Investigation: A.R.-N, B.K., F.F.; Writing - original draft: M.J.A.; Writing - review & editing: A.R.-N, F.F., G.R., C.D., M.J.A.; Supervision: M.J.A.; Funding acquisition: M.J.A.

Funding

This project and B.K. are supported by the project grant awarded by the Fundação para a Ciência e a Tecnologia (FCT) (Portugal: PTDC/IMI-MIC/1142/2012). M.J.A. is funded by the FCT investigator fellowship IF/00899/2013; M.A. and S.V.-C. by the FCT postdoc fellowships (SFRH/BPD/62982/2009 and SFRH/BPD/94204/2013, respectively); F.F. by the Instituto and Fundação Calouste Gulbenkian, Portugal. G.R. is supported by Fondation pour la Recherche Médicale (Equipe FRM DEQ20140329491 Team label), C.D. by the Fondation ARC pour la Recherche sur le Cancer (PJA20161204965), and both by Centre National de la Recherche Scientifique (CNRS), Institut National de la Santé et de la Recherche Médicale (INSERM) and Institut Curie.

Supplementary information

Supplementary information available online at
http://jcs.biologists.org/lookup/doi/10.1242/jcs.210807.supplemental

References

Amorim, M. J., Bruce, E. A., Read, E. K. C., Foeglein, A., Mahen, R., Stuart, A. D. and Digard, P. (2011). A Rab11- and microtubule-dependent mechanism for cytoplasmic transport of influenza A virus viral RNA. *J. Virol.* **85**, 4143-4156.

Amorim, M. J., Kao, R. Y. and Digard, P. (2013). Nucleozin targets cytoplasmic trafficking of viral ribonucleoprotein-rab11 complexes in influenza a virus infection. *J. Virol.* **87**, 4694-4703.

Arranz, R., Coloma, R., Chichon, F. J., Conesa, J. J., Carrascosa, J. L., Valpuesta, J. M., Ortin, J. and Martin-Benito, J. (2012). The structure of native influenza virion ribonucleoproteins. *Science* **338**, 1634-1637.

Avalos, R. T., Yu, Z. and Nayak, D. P. (1997). Association of influenza virus NP and M1 proteins with cellular cytoskeletal elements in influenza virus-infected cells. *J. Virol.* **71**, 2947-2958.

Avilov, S. V., Moisy, D., Naffakh, N. and Cusack, S. (2012). Influenza A virus progeny vRNP trafficking in live infected cells studied with the virus-encoded fluorescently tagged PB2 protein. *Vaccine* **30**, 7411-7417.

Badding, M. A. and Dean, D. A. (2013). Highly acetylated tubulin permits enhanced interactions with and trafficking of plasmids along microtubules. *Gene Ther.* **20**, 616-624.

Bruce, E. A., Digard, P. and Stuart, A. D. (2010). The Rab11 pathway is required for influenza A virus budding and filament formation. *J. Virol.* **84**, 5848-5859.

Chen, B. J., Leser, G. P., Jackson, D. and Lamb, R. A. (2008). The influenza virus M2 protein cytoplasmic tail interacts with the M1 protein and influences virus assembly at the site of virus budding. *J. Virol.* **82**, 10059-10070.

Chou, Y.-Y., Heaton, N. S., Gao, Q., Palese, P., Singer, R. and Lionnet, T. (2013). Colocalization of different influenza viral RNA segments in the cytoplasm before viral budding as shown by single-molecule sensitivity FISH analysis. *PLoS Pathog.* **9**, e1003358.

de Wit, E., Spronken, M. I. J., Bestebroer, T. M., Rimmelzwaan, G. F., Osterhaus, A. D. M. E. and Fouchier, R. A. M. (2004). Efficient generation and growth of influenza virus A/PR/8/34 from eight cDNA fragments. *Virus Res.* **103**, 155-161.

Delevoye, C., Hurbain, I., Tenza, D., Sibarita, J.-B., Uzan-Gafsou, S., Ohno, H., Geerts, W. J. C., Verkleij, A. J., Salamero, J., Marks, M. S. et al. (2009). AP-1 and KIF13A coordinate endosomal sorting and positioning during melanosome biogenesis. *J. Cell Biol.* **187**, 247-264.

Delevoye, C., Miserey-Lenkei, S., Montagnac, G., Gilles-Marsens, F., Paul-Gilloteaux, P., Giordano, F., Waharte, F., Marks, M. S., Goud, B. and Raposo, G. (2014). Recycling endosome tubule morphogenesis from sorting endosomes requires the kinesin motor KIF13A. *Cell Rep* **6**, 445-454.

Digard, P., Elton, D., Bishop, K., Medcalf, E., Weeds, A. and Pope, B. (1999). Modulation of nuclear localization of the influenza virus nucleoprotein through interaction with actin filaments. *J. Virol.* **73**, 2222-2231.

Doms, R. W., Lamb, R. A., Rose, J. K. and Helenius, A. (1993). Folding and assembly of viral membrane proteins. *Virology* **193**, 545-562.

Eisfeld, A. J., Kawakami, E., Watanabe, T., Neumann, G. and Kawaoka, Y. (2011). RAB11A is essential for transport of the influenza virus genome to the plasma membrane. *J. Virol.* **85**, 6117-6126.
Eisfeld, A. J., Neumann, G. and Kawaoka, Y. (2015). At the centre: influenza A virus ribonucleoproteins. *Nat. Rev. Microbiol.* **13**, 28-41.
Elton, D., Simpson-Holley, M., Archer, K., Medcalf, L., Hallam, R., Mccauley, J. and Digard, P. (2001). Interaction of the influenza virus nucleoprotein with the cellular CRM1-mediated nuclear export pathway. *J. Virol.* **75**, 408-419.
Fan, G.-H., Lapierre, L. A., Goldenring, J. R., Sai, J. and Richmond, A. (2004). Rab11-family interacting protein 2 and myosin Vb are required for CXCR2 recycling and receptor-mediated chemotaxis. *Mol. Biol. Cell* **15**, 2456-2469.
Fournier, E., Moules, V., Essere, B., Paillart, J.-C., Sirbat, J.-D., Isel, C., Cavalier, A., Rolland, J.-P., Thomas, D., Lina, B. et al. (2012). A supramolecular assembly formed by influenza A virus genomic RNA segments. *Nucleic Acids Res.* **40**, 2197-2209.
Gerber, M., Isel, C., Moules, V. and Marquet, R. (2014). Selective packaging of the influenza A genome and consequences for genetic reassortment. *Trends Microbiol.* **22**, 446-455.
Giese, S., Bolte, H. and Schwemmle, M. (2016). The feat of packaging eight unique genome segments. *Viruses* **8**, 165.
Gramlich, M. W., Conway, L., Liang, W. H., Labastide, J. A., King, S. J., Xu, J. and Ross, J. L. (2017). Single molecule investigation of Kinesin-1 motility using engineered microtubule defects. *Sci. Rep.* **7**, 44290.
Horgan, C. P. and Mccaffrey, M. W. (2009). The dynamic Rab11-FIPs. *Biochem. Soc. Trans.* **37**, 1032-1036.
Husain, M. and Harrod, K. S. (2011). Enhanced acetylation of alpha-tubulin in influenza A virus infected epithelial cells. *FEBS Lett.* **585**, 128-132.
Hutchinson, E. C., von Kirchbach, J. C., Gog, J. R. and Digard, P. (2010). Genome packaging in influenza A virus. *J. Gen. Virol.* **91**, 313-328.
Hutchinson, E. C., Charles, P. D., Hester, S. S., Thomas, B., Trudgian, D., Martínez-Alonso, M. and Fodor, E. (2014). Conserved and host-specific features of influenza virion architecture. *Nat. Commun.* **5**, 4816.
Kao, R. Y., Yang, D., Lau, L.-S., Tsui, W. H. W., Hu, L., Dai, J., Chan, M.-P., Chan, C.-M., Wang, P., Zheng, B.-J. et al. (2010). Identification of influenza A nucleoprotein as an antiviral target. *Nat. Biotechnol.* **28**, 600-605.
Kawaguchi, A., Hirohama, M., Harada, Y., Osari, S. and Nagata, K. (2015). Influenza virus induces cholesterol-enriched endocytic recycling compartments for budozone formation via cell cycle-independent centrosome maturation. *PLoS Pathog.* **11**, e1005284.
Lakdawala, S. S., Wu, Y., Wawrzusin, P., Kabat, J., Broadbent, A. J., Lamirande, E. W., Fodor, E., Altan-Bonnet, N., Shroff, H. and Subbarao, K. (2014). Influenza a virus assembly intermediates fuse in the cytoplasm. *PLoS Pathog.* **10**, e1003971.
Lakdawala, S. S., Fodor, E. and Subbarao, K. (2016). Moving on out: transport and packaging of influenza viral RNA into virions. *Annu. Rev. Virol.* **3**, 411-427.
Lapierre, L. A., Kumar, R., Hales, C. M., Navarre, J., Bhartur, S. G., Burnette, J. O., Provance, D. W., Jr, Mercer, J. A., Bahler, M. and Goldenring, J. R. (2001). Myosin vb is associated with plasma membrane recycling systems. *Mol. Biol. Cell* **12**, 1843-1857.
Ma, K., Roy, A.-M. M. and Whittaker, G. R. (2001). Nuclear export of influenza virus ribonucleoproteins: identification of an export intermediate at the nuclear periphery. *Virology* **282**, 215-220.
Matrosovich, M., Matrosovich, T., Garten, W. and Klenk, H.-D. (2006). New low-viscosity overlay medium for viral plaque assays. *Virol. J.* **3**, 63.
Momose, F., Kikuchi, Y., Komase, K. and Morikawa, Y. (2007). Visualization of microtubule-mediated transport of influenza viral progeny ribonucleoprotein. *Microbes Infect.* **9**, 1422-1433.
Momose, F., Sekimoto, T., Ohkura, T., Jo, S., Kawaguchi, A., Nagata, K. and Morikawa, Y. (2011). Apical transport of influenza A virus ribonucleoprotein requires Rab11-positive recycling endosome. *PLoS ONE* **6**, e21123.
Nakagawa, T., Setou, M., Seog, D.-H., Ogasawara, K., Dohmae, N., Takio, K. and Hirokawa, N. (2000). A novel motor, KIF13a, transports mannose-6-phosphate receptor to plasma membrane through direct interaction with AP-1 complex. *Cell* **103**, 569-581.
Noda, T. and Kawaoka, Y. (2010). Structure of influenza virus ribonucleoprotein complexes and their packaging into virions. *Rev. Med. Virol.* **20**, 380-391.
Noton, S. L., Medcalf, E., Fisher, D., Mullin, A. E., Elton, D. and Digard, P. (2007). Identification of the domains of the influenza A virus M1 matrix protein required for NP binding, oligomerization and incorporation into virions. *J. Gen. Virol.* **88**, 2280-2290.
Nturibi, E., Bhagwat, A. R., Coburn, S., Myerburg, M. M. and Lakdawala, S. S. (2017). Intracellular colocalization of influenza viral RNA and Rab11A is dependent upon microtubule filaments. *J. Virol.* **91**, e01179-17.
Perez Bay, A. E., Schreiner, R., Mazzoni, F., Carvajal-Gonzalez, J. M., Gravotta, D., Perret, E., Lehmann Mantaras, G., Zhu, Y.-S. and Rodriguez-Boulan, E. J. (2013). The kinesin KIF16B mediates apical transcytosis of transferrin receptor in AP-1B-deficient epithelia. *EMBO J.* **32**, 2125-2139.
Pflug, A., Guilligay, D., Reich, S. and Cusack, S. (2014). Structure of influenza A polymerase bound to the viral RNA promoter. *Nature* **516**, 355-360.
Provance, D. W., Jr., Addison, E. J., Wood, P. R., Chen, D. Z., Silan, C. M. and Mercer, J. A. (2008). Myosin-Vb functions as a dynamic tether for peripheral endocytic compartments during transferrin trafficking. *BMC Cell Biol.* **9**, 44.
Roberts, P. C. and Compans, R. W. (1998). Host cell dependence of viral morphology. *Proc. Natl. Acad. Sci. USA* **95**, 5746-5751.
Roland, J. T., Bryant, D. M., Datta, A., Itzen, A., Mostov, K. E. and Goldenring, J. R. (2011). Rab GTPase-Myo5B complexes control membrane recycling and epithelial polarization. *Proc. Natl. Acad. Sci. USA* **108**, 2789-2794.
Schonteich, E., Wilson, G. M., Burden, J., Hopkins, C. R., Anderson, K., Goldenring, J. R. and Prekeris, R. (2008). The Rip11/Rab11-FIP5 and kinesin II complex regulates endocytic protein recycling. *J. Cell Sci.* **121**, 3824-3833.
Shaw, M. L., Stone, K. L., Colangelo, C. M., Gulcicek, E. E. and Palese, P. (2008). Cellular proteins in influenza virus particles. *PLoS Pathog.* **4**, e1000085.
Simpson-Holley, M., Ellis, D., Fisher, D., Elton, D., Mccauley, J. and Digard, P. (2002). A functional link between the actin cytoskeleton and lipid rafts during budding of filamentous influenza virions. *Virology* **301**, 212-225.
Sugita, Y., Sagara, H., Noda, T. and Kawaoka, Y. (2013). Configuration of viral ribonucleoprotein complexes within the influenza A virion. *J. Virol.* **87**, 12879-12884.
Sun, E., He, J. and Zhuang, X. (2013). Dissecting the role of COPI complexes in influenza virus infection. *J. Virol.* **87**, 2673-2685.
Vale-Costa, S. and Amorim, M. J. (2016a). Clustering of Rab11 vesicles in influenza A virus infected cells creates hotspots containing the eight viral ribonucleoproteins. *Small GTPases* **8**, 71-77.
Vale-Costa, S. and Amorim, M. J. (2016b). Recycling endosomes and viral infection. *Viruses* **8**, 64.
Vale-Costa, S., Alenquer, M., Sousa, A. L., Kellen, B., Ramalho, J., Tranfield, E. M. and Amorim, M. J. (2016). Influenza A virus ribonucleoproteins modulate host recycling by competing with Rab11 effectors. *J. Cell Sci.* **129**, 1697-1710.
Verdeny-Vilanova, I., Wehnekamp, F., Mohan, N., Sandoval Alvarez, A., Borbely, J. S., Otterstrom, J. J., Lamb, D. C. and Lakadamyali, M. (2017). 3D motion of vesicles along microtubules helps them to circumvent obstacles in cells. *J. Cell Sci.* **130**, 1904-1916.
Welz, T., Wellbourne-Wood, J. and Kerkhoff, E. (2014). Orchestration of cell surface proteins by Rab11. *Trends Cell Biol.* **24**, 407-415.
Xiong, B., Bayat, V., Jaiswal, M., Zhang, K., Sandoval, H., Charng, W.-L., Li, T., David, G., Duraine, L., Lin, Y.-Q. et al. (2012). Crag is a GEF for Rab11 required for rhodopsin trafficking and maintenance of adult photoreceptor cells. *PLoS Biol.* **10**, e1001438.
Yamayoshi, S., Watanabe, M., Goto, H. and Kawaoka, Y. (2015). Identification of a novel viral protein expressed from the PB2 segment of influenza A virus. *J. Virol.* **90**, 444-456.